applied sciences

MDPI

Article

Performance Evaluation of Grounding Systems of Medium-Voltage Concrete Poles: A Comprehensive Analysis

Emmanouil D. Ellinas, Georgios Lianos, Vassiliki T. Kontargyri *, Christos A. Christodoulou and Ioannis F. Gonos

School of Electrical & Computer Engineering, National Technical University of Athens, 15780 Zografou Attica, Greece; manellhnas@central.ntua.gr (E.D.E.); el11516@central.ntua.gr (G.L.); christodoulou@power.ece.ntua.gr (C.A.C.); igonos@cs.ntua.gr (I.F.G.)
* Correspondence: vkont@power.ece.ntua.gr

Featured Application: The paper investigates the efficacy of grounding systems in power distribution networks during the transition from overhead to underground network configurations. Through scenario analysis and comparative evaluations, it aims to provide insights for optimal design methodologies, emphasizing safety and techno-economic criteria. Factors such as soil structure, fault current magnitude, and fault clearing times are examined to standardize the design of grounding systems in distribution networks.

Abstract: Designing and installing efficient grounding systems in power distribution networks is considered a complex and crucial task to ensure the reliable operation of power-protective schemes while mitigating hazardous potentials arising from faults, thereby safeguarding both personnel and equipment. This paper aims to offer guidance on designing effective grounding systems in distribution networks by assessing the influence of parameters such as soil structure, fault current magnitude, and fault clearing time. This involves proposing a more precise methodology for calculating hazardous potentials, leveraging software tools like PowerFactory, to accurately determine short-circuit (SC) currents and fault clearing times at specific locations where grounding grids are to be installed. Consequently, Distribution System Operators (DSOs) can design tailored grounding systems that optimize techno-economic considerations without unnecessary over-dimensioning, accounting for the unique characteristics of the Medium-Voltage (MV) Line and soil structure.

Keywords: grounding systems; distribution network; short-circuit analysis; renewable energy sources

Citation: Ellinas, E.D.; Lianos, G.; Kontargyri, V.T.; Christodoulou, C.A.; Gonos, I.F. Performance Evaluation of Grounding Systems of Medium-Voltage Concrete Poles: A Comprehensive Analysis. *Appl. Sci.* **2024**, *14*, 3758. https://doi.org/10.3390/app14093758

Academic Editor: Alessandro Lo Schiavo

Received: 29 February 2024
Revised: 23 April 2024
Accepted: 26 April 2024
Published: 28 April 2024

1. Introduction

The evolving landscape of power distribution networks necessitates a thorough investigation into grounding systems with a particular focus on the unique challenges posed by complex network configurations featuring the transition from overhead power lines to underground cables. Grounding systems play a key role in ensuring the reliability of power distribution networks by facilitating protective measures, mitigating potential hazards, and ensuring the safety of personnel and equipment. Nowadays, power grids evolve continuously due to the increased global electricity demands, the proliferation of renewable energy sources, and the increased frequency of extreme weather incidents. To illustrate this further, according to [1] the electrification of various sectors such as transportation and heating will continue to persist and, therefore, a projected annual increase of approximately 2% in global electricity demand is anticipated until 2025, as depicted in Figure 1 [1].

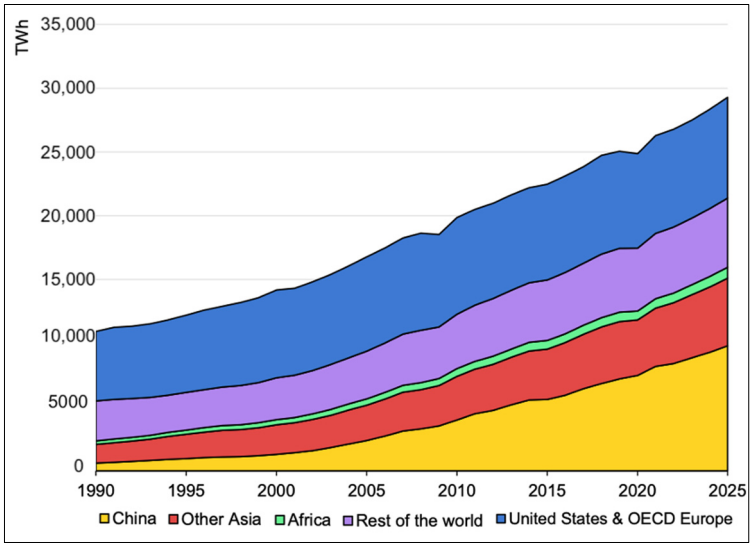

Figure 1. Evolution of global electricity demand by region [1].

Regarding the integration of renewable energy sources into power grids, 2023 witnessed a substantial surge in global capacity, with an addition of approximately 107 gigawatts (GW) representing the most significant increase ever recorded [2,3]. Figure 2 illustrates the anticipated electricity generation from various renewable energy sources in the future, showcasing an upward trajectory in the generation levels. This growth is being driven by the global policy to minimize the use of fossil fuels and reduce net greenhouse gas emissions by at least 55% by 2030 and 100% by 2050 [2–4].

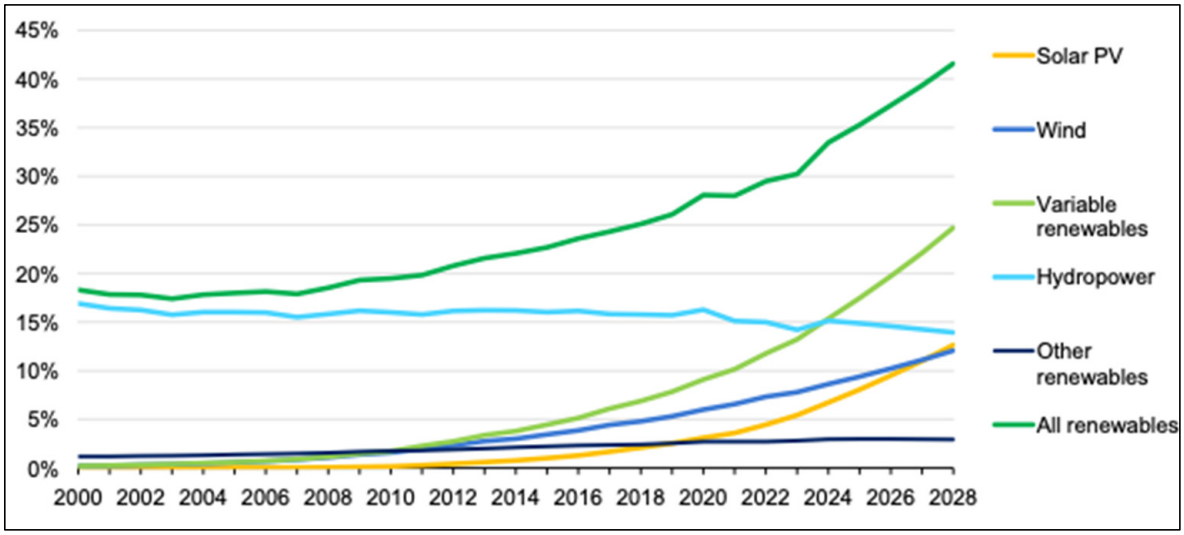

Figure 2. Electricity generation by technology, 2000–2028 [2].

In this context, emphasis is placed on modernizing and reinforcing power distribution networks. Within this framework, the need to analyze and optimize the performance of grounding systems in MV power networks becomes a task of high importance. This significance stems from the critical role grounding systems play in ensuring the reliability of power networks, as their efficient operation directly influences the networks' stability. In more detail, these systems act as a crucial link in the protective chain, serving to maintain the networks' operational integrity, minimize risks associated with fault occurrences, and ensure the safety of personnel and equipment [5,6].

The modernization of power distribution networks often involves a transition from traditional overhead configurations to underground setups. This shift is driven by fac-

tors such as aesthetic considerations, environmental concerns, and the need for enhanced resilience to extreme weather conditions. Reinforced concrete poles serve as key components in facilitating this transition, providing a robust connection between overhead and underground systems using disconnect switches [7,8].

Over the years, extensive research has been conducted, and numerous guidelines have been published, regarding the design of grounding systems, particularly focusing on High-Voltage/Medium-Voltage (HV/MV) substations and renewable energy sources such as wind farms and photovoltaic parks. In fact, refs. [9,10] intend to offer guidance and relevant information regarding safe grounding practices focused on AC substations and a section in [11] describes, concisely, the fundamental requirements of the design, installation, testing, and maintenance of an earthing system of High-Voltage (HV) and Low-Voltage (LV) systems. Additionally, ref. [12] provides basic guidance on the effects of shock current on human beings and livestock. Moreover, in [13] the influence of the renewable energy sources on the grounding method of the neutral point of the HV transformer is studied and in [14] several factors of neutral grounding are analyzed in an effort to highlight their influence on the reliable operation of power distribution networks. Furthermore, in [15] fundamental aspects, definitions, and best practices regarding earthing systems in HV substations are outlined and in [16] a method for the straightforward safety assessment of typical grounding configurations of Medium-Voltage/Low-Voltage (MV/LV) substations is introduced on the basis of simple calculations. Additionally, a mathematical and numerical formulation, based on the well-known Maxwell's Equations, is developed to design and analyze grounding systems in underground electrical substations and it is presented in [17,18]; emphasis is given to evaluating the grounding system for an underground distribution substation using a modified average potential method. Finally, in [19] a numerical model based on the boundary element method allows the analysis of the grounding systems of aboveground and underground substations under different locations and considerations.

Despite the aformentioned literature which is mainly focused on the study of grounding in HV/MV substations, there has been relatively little research conducted on the earthing systems of power distribution lines.

Within the [20], specific provisions detail the safety thresholds that grounding grids must meet and, as a result, Distribution System Operators (DSOs) are tasked with developing grounding grid designs that adhere to these specified criteria. A crucial aspect of the study procedure of grounding systems of MV lines is the absence of guidelines governing their design and operation. This lack of uniformity highlights the complexity and multifaceted nature of the challenges encountered in optimizing grounding systems, necessitating a detailed and context-specific analysis [5–8]. In this framework, the current paper aims to analyze and optimize grounding systems by investigating several crucial parameters, encompassing soil structure, fault current magnitude, fault clearing times, and other operational variables that influence grounding system performance. To this end, a typical MV line, including its entire protection scheme, will be simulated using the DIgSILENT PowerFactory software tool. Short-circuit currents resulting from single-line-to-ground faults will be calculated, accounting for distributed generation (DG) units with varying rated power outputs and installation locations across the MV line. Evaluation of the grounding system's performance will be conducted for each fault scenario, leveraging the extensive capabilities offered by the SES CDEGS 19.0 software tool. It is noteworthy that this evaluation will encompass diverse soil structures and fault clearing times in accordance with the Time–Current Curves (TCCs) of the network's protection devices.

In summary, this study aims to provide practical insights into how different parameters influence grounding system performance, thereby enhancing safety and efficiency within power distribution networks. However, achieving the optimal design of grounding systems extends beyond technical considerations alone; it necessitates addressing safety concerns while also aligning with techno-economic criteria. Balancing safety with economic feasibility is recognized as a crucial aspect in developing grounding systems that

not only meet operational demands but also contribute to the overall sustainability of Medium-Voltage networks.

2. Simulation Models

2.1. Medium-Voltage Power Line

This paper presents a simulated 20 km, 20 kV power line incorporating Distributed Generation (DG), as depicted in Figure 3. The Single-Line Diagram (SLD) illustrates three distinct voltage levels, each one of them denoted by different a color: namely, HV (150 kV), Medium Voltage (20 kV), and Low Voltage (400 V). The distribution network has a three-phase, three-wire configuration, with grounding implemented at the sending end of the HV/MV substation via a 12 Ohm resistance, restricting single-line-to-ground faults to a maximum of 1000 A. Detailed information regarding the key characteristics of the MV line is provided in Tables 1–4.

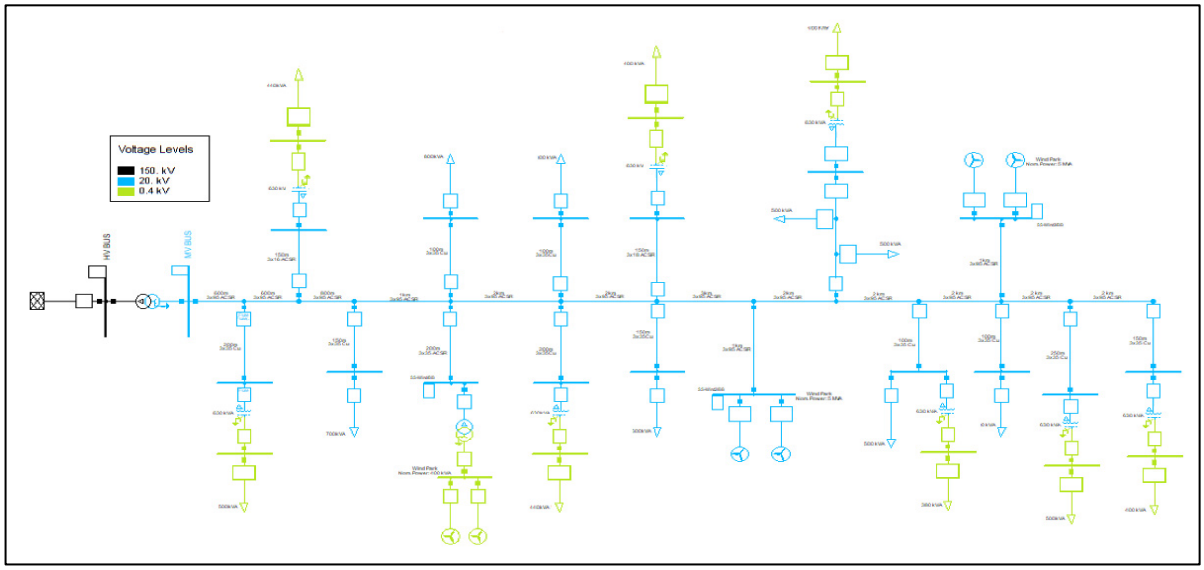

Figure 3. Medium-voltage line model.

Table 1. Infinite HV Line Model Characteristics.

Characteristics	Maximum Value	Minimum Value
Short-circuit Power S_k''	8054 MVA	7794 MVA
Short-circuit Current I_k''	31 kA	30 kA
R/X ratio	0.1	0.1
Z_2/Z_1	1	1
X_2/X_1	1	1
R_2/X_0	0.1	0.1

Table 2. HV/MV Transformer Characteristics.

Characteristics	Maximum Value
Rated Power	50 MVA
Frequency	50 Hz
High-Voltage side	150 kV
Low-Voltage side	20 kV
Short-Circuit Voltage U_k	20%
Short-Circuit Voltage U_{k0}	20%
Vector Group	Dyn1
Neutral Resistance R_c	12 Ω

Table 3. Conductor Characteristics.

Conductor Type	I_{max} (A)	Single-Line-to-Ground Fault Resistance, R_{1f} (Ω/km)	Single-Line-to-Ground Fault Reactance, X_{1f} (Ω/km)
3 × 95 ASCR	448	0.264	0.741
3 × 50 ASCR	296	0.453	0.785
3 × 35 ASCR	224	0.625	0.796
3 × 50 Cu	232	0.475	0.785
3 × 35 Cu	285	0.645	0.8

Table 4. MV/LV transformer characteristics.

Transformer Nominal Power (kVA)	Short-Circuit Voltage U_k (%)	Short-Circuit Voltage U_{k0} (%)	Vector Group
100	4	3	Yzn11
250	4	3	Dyn11
400	4	3	Dyn11
630	4	3	Dyn11
1000	6	3	Dyn11

The protection scheme for the modeled MV line in Figure 3 comprises several components [21]:

1. A Current Transformer (CT), an overcurrent relay, and a Circuit Breaker (CB) are included. The CT monitors the main feeder, while the overcurrent relay and CB are designed to promptly identify and safely clear any short-circuits within the distribution network.
2. Branches along the line, where compact substations are installed, are safeguarded by fuse cut-outs (T-Type Fuses).

For the purposes of this paper, the ABB REF 615 relay's definite time and extremely inverse overcurrent elements (51P, 50P1, 51N, and 50N function blocks) are modeled using the DIgSILENT PowerFactory 2022 software tool. The reclosing operational sequence of the CB involves one instantaneous operation and three time delays (TDs). The instantaneous operation of the CB is set to 0.15 s, and the time delays are determined based on the IEC Extremely Inverse Time–Current Characteristic (TCC) [22–25]. As it is presented in Figure 4, CB's reclosing operational sequence is set to one instantaneous operation and three TDs.

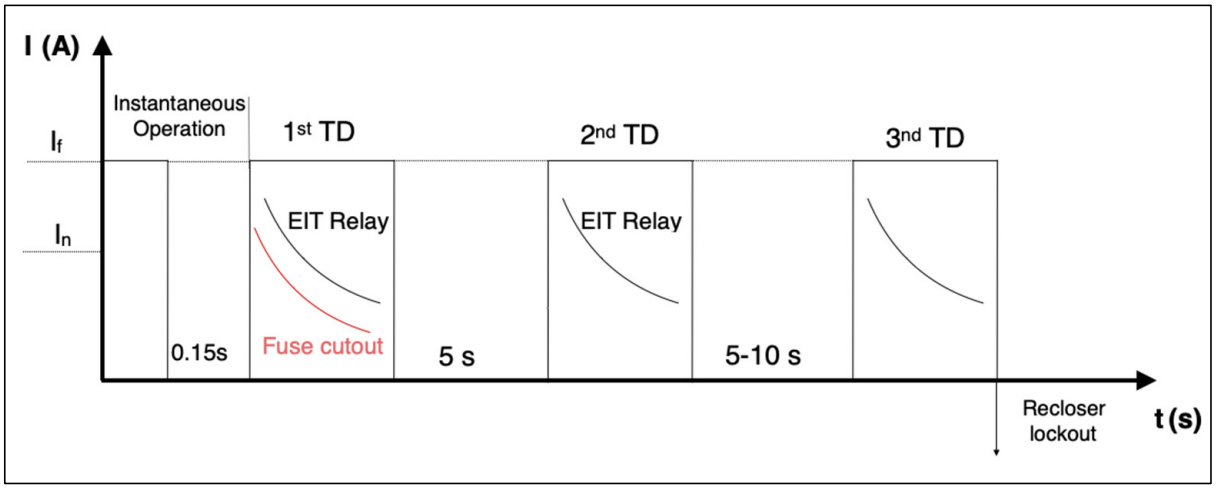

Figure 4. Operational sequence of an overcurrent relay.

The instantaneous operation of the CB is set to 0.15 s and the TDs are set according to IEC 60255 Extremely Inverse Time (EIT)–Current Characteristic by selecting $\alpha = 2$, TD = 0.7, and a pickup current of 80 A described by the Equation (1) [22–25]:

$$t = \frac{k \times B}{\left(\frac{I}{I_s}\right)^a - 1} \tag{1}$$

The corresponding EIT–Current Characteristic of the CB and the fuses is depicted in Figure 5. The chosen fuses for branch protection are the 30 T type. To ensure proper coordination between the Circuit Breaker of the main feeder and the fuse cut-outs of the branches, the relevant TCCs should have a minimum separation of 0.4 s. This arrangement guarantees that, in the event of a SC in one of the branches of the MV line, the smallest possible segment of the network will be isolated [26].

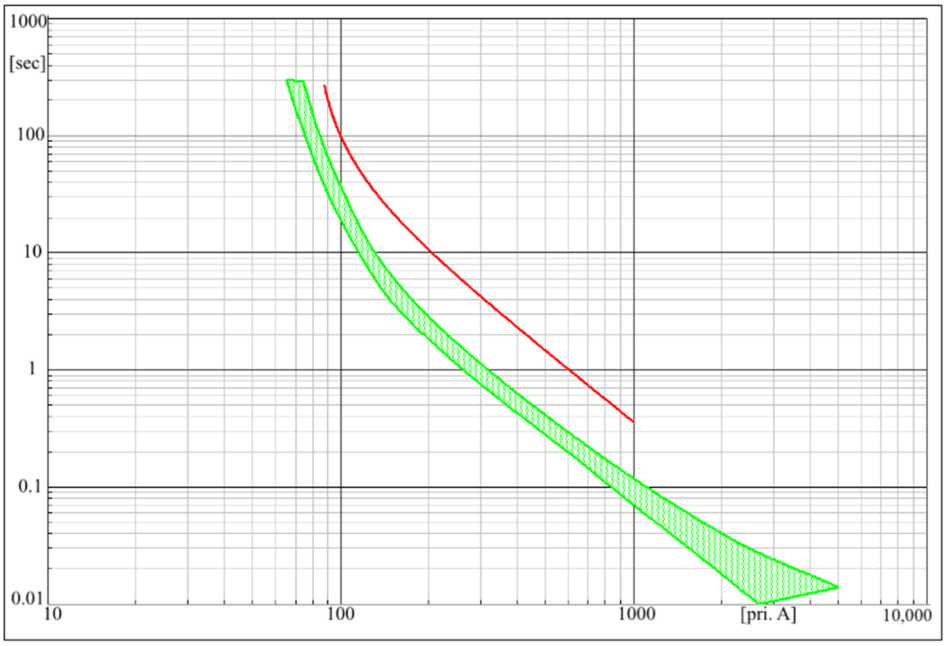

Figure 5. Protection coordination TCCs (Green: Fuse cut-outs, Red: Overcurrent Relay).

2.2. Grounding Grid Models

This study investigates three variations of a grounding grid. To further elaborate, all three grids are constructed by 35 mm^2 copper, consisting of two main sections. The initial section comprises a meshed square grid (1.2 × 1.2 m) positioned 0.3 m beneath the Earth's surface, while the second section involves a circular conductor positioned at the same depth, connected with the square section via copper. The grounding grid configurations, identified as Grids A, B, and C, are depicted in Figure 6. Specifically, Grid A serves as the foundational grounding grid, while in Grid B, the radius of the circular loop is increased by 50%. Additionally, Grid C incorporates a vertical rod when compared to Grid A and B. The primary objective is to mitigate touch and step voltages during SC occurrences, ensuring adherence to specified safety thresholds outlined in [9]. These values shall not exceed the limits, defined by the below-mentioned equations for a body of 70 kg [9]:

$$E_{step70} = (1000 + 6C_s \cdot \rho_s)\frac{0.157}{\sqrt{t_s}} \tag{2}$$

$$E_{touch70} = (1000 + 1.5C_s \cdot \rho_s)\frac{0.157}{\sqrt{t_s}} \tag{3}$$

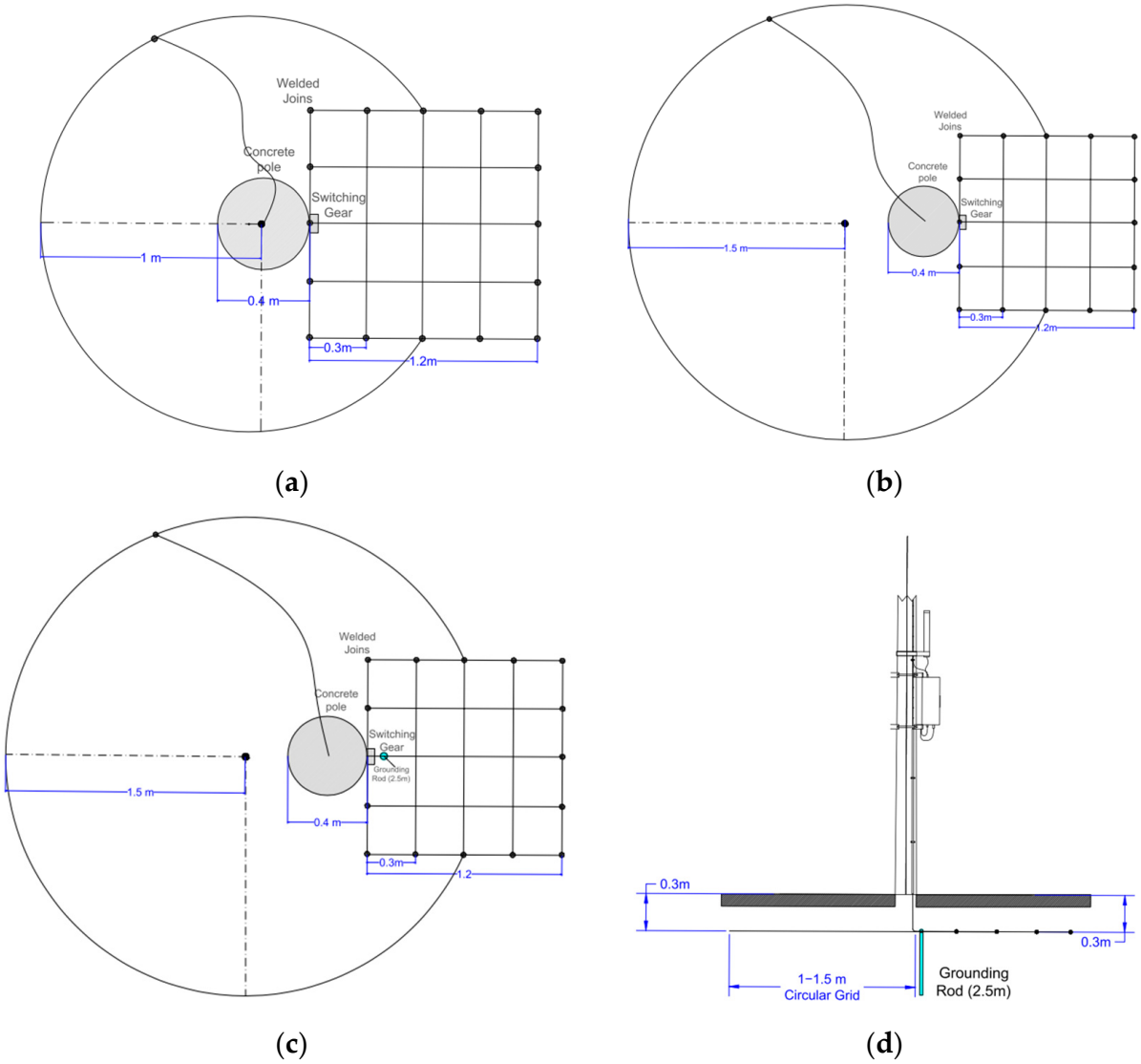

Figure 6. Grounding grid variations: (**a**) Grid A: top view of meshed grid with 1 m radius circular conductor, (**b**) Grid B: top view of meshed grid with 1.5 m radius circular conductor, (**c**) Grid C: top view of meshed grid with 1.5 m radius circular conductor with the addition of 1 vertical rod underneath the concrete pole, and (**d**) side view of Grounding Grid C.

The safety threshold for a person weighing 70 kg approaching a faulty area is marginally higher than for someone weighing 50 kg. Consequently, the scenario involving a 70 kg individual has been modeled as a best-case scenario. In the case that safety thresholds are not met in this case, they will not be met in the case of a 50 kg individual as well. The latter could be a subject of future research.

The safety thresholds for touch and step voltages are automatically calculated by the SES CDEGS 19.0 software tool for each simulated scenario. However, according to [9], the values of Cs are determined using the following empirical equation:

$$C_s = 1 - \frac{0.09 \cdot \left(1 - \frac{\rho}{\rho_s}\right)}{2 \cdot h_s + 0.09}$$

where:

ρ_s is the resistivity of the surface material in Ω-m,
ρ is the soil resistivity in Ω-m,

h_s is the thickness of surface material in m.

The value of t_s represents the fault clearing time for each scenario utilized, determined by the operational sequence of the overcurrent relay depicted in Figures 4 and 5.

3. Methodology

To assess the performance of the aforementioned variations of grounding grids and to compare them with the safety measures and criteria mentioned in [9], several scenarios were taken into consideration. To further elaborate, extensive simulations were undertaken, encompassing grounding grids with diverse configurations (as depicted in Figure 6), alongside variations in soil models and resistivity. In more detail:

- A uniform soil structure and a horizontal two-layer soil model with h = 1 m the depth of the first layer was applied to all three variations;
- This study investigates the variability of soil resistivity across power distribution grid routes. Although power distribution grid routes traverse mainly farmland regions, characterized by resistivity values typically ranging from 100 to 300 Ωm, for research purposes, a wider range of soil resistivity scenarios were studied. These scenarios included uniform resistivity values ranging from 15 Ωm to 1000 Ωm, as well as horizontal two-layer soil models [27,28]. In the latter, the resistivity of the first layer varied from 100 Ωm to 1000 Ωm, while the resistivity of the second layer ranged from 100 Ωm to 2000 Ωm;
- The total resistance of the grounding grid was calculated for each soil resistivity using the SES CDEGS software tool [27,28];
- This study explores potential installation sites for the MV concrete pole, assessing three distinct scenarios: near the HV/MV substation (L = 0 km), at the middle of the MV line (L = 10 km), and at the end of it (L = 20 km);
- For each installation location mentioned above, the maximum single-line-to-ground fault current was determined using the PowerFactory 2022 software tool; the magnitude of the single-line-to-ground fault is contingent upon four resistances arranged in series, as illustrated in the Figure 7 and described in Equation (4) [26]:

$$I_{1f} = \frac{V_f}{\sqrt{\left(R_f \cdot l + R_N + R_G\right)^2 + \left(X_f \cdot l + X_T\right)^2}} \quad (4)$$

where:

I_{1f}: Single-line-to-ground fault
V_f: Line-to-ground voltage
R_G: Grounding grid's total resistance (depending on the soil resistivity)
R_N: Neutral point of the HV transformer resistance
R_f: Equivalent single-line-to-ground fault resistance of 95 ACSR Conductor
X_f: Equivalent single-line-to-ground fault impedance of 95 ACSR Conductor
X_T: HV transformer impedance

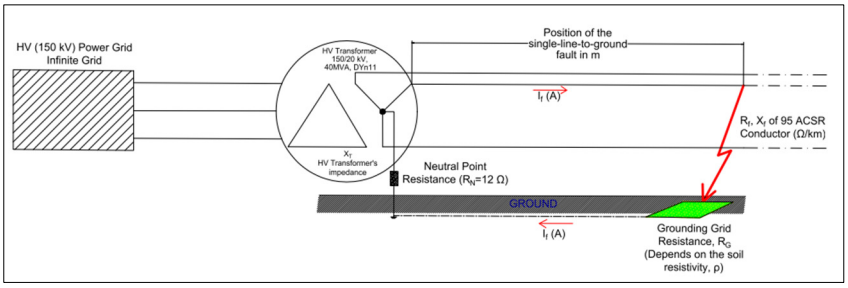

Figure 7. Single-line-to-ground fault current path.

- Regarding fault clearing time, the instantaneous operation of the circuit breaker (CB) with a time of 0.15 s for the MV line was selected.

The adopted procedure for the analysis is presented in Figure 8.

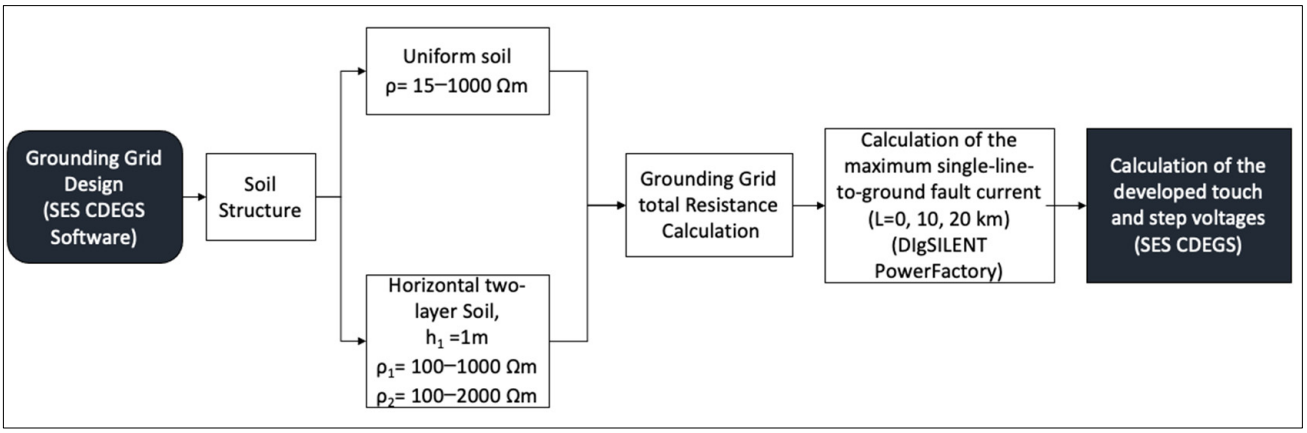

Figure 8. Study of the grounding grids flow chart.

4. Results

This section presents the results derived from the SC analysis performed using the PowerFactory software tool. Furthermore, it includes graphs illustrating the touch and step voltage levels across the grounding systems in the event of a fault. The analysis incorporates parameters such as a soil resistivity of 300 Ωm (common value for farmlands), a pole position situated 10 km away from the HV/MV substation, and a fault clearing time of 0.15 s, indicative of transient faults. The graphs of the hazardous potentials have been generated using the SES CDEGS plotting and reporting module [27].

4.1. Short-Circuit Current Analysis

Figure 9 showcases the distribution of SC currents along the MV line. The magnitude of these currents is contingent not only upon the fault's location but also upon its total resistance. Specifically, short-circuits in proximity to the HV/MV substation yield higher fault magnitudes than the ones at the end of the line. Furthermore, it is noteworthy that single-line-to-ground faults tend asymptotically to a specific value as the grounding grid's resistance increases. Additionally, the discrepancy in magnitude ($\Delta I = I2 - I1$) between short-circuits, with the same grounding grid resistance but occurring at distinct line locations, diminishes while the resistance increases. The minimum asymptotic value of the SC current approximates 80 A at a soil resistivity of 1000 Ωm, while for even higher resistivity, the minimum SC current may reach even lower. Consequently, circuit breakers are configured with at least a pickup current set of 80 A to ensure the clearance of such low-magnitude fault currents. In Figure 8, *R* value represents the coefficient of determination factor that measures the strength of the relationship between the model and the dependent variable on a 0–100% scale.

4.2. Developed Potentials on the Grounding System

Figure 10 illustrates the total resistance of each grounding grid as a function of the soil resistivity (ρ = 15–1000 Ωm). According to the figure, we can safely conclude that there exists a linear relation between the total resistance of the grounding grids and the soil resistivity in the case of uniform soil resistivity; however, this is not the case in the horizontal two-layer soil structure.

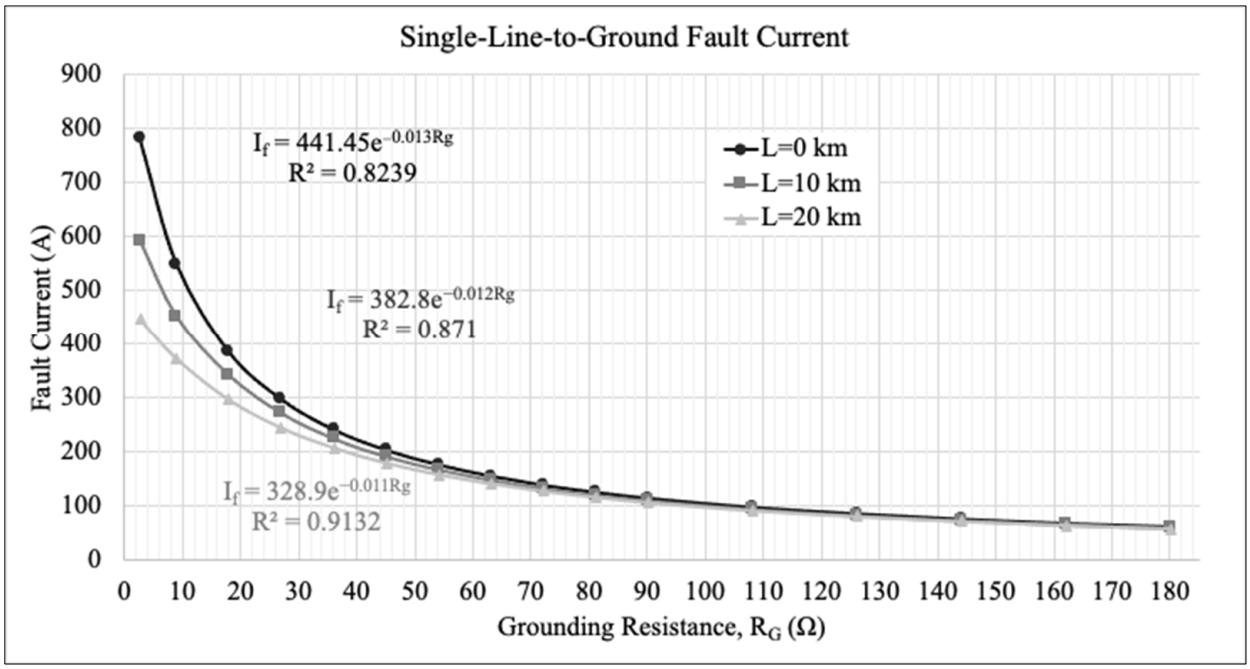

Figure 9. Single-line-to-ground fault current distribution.

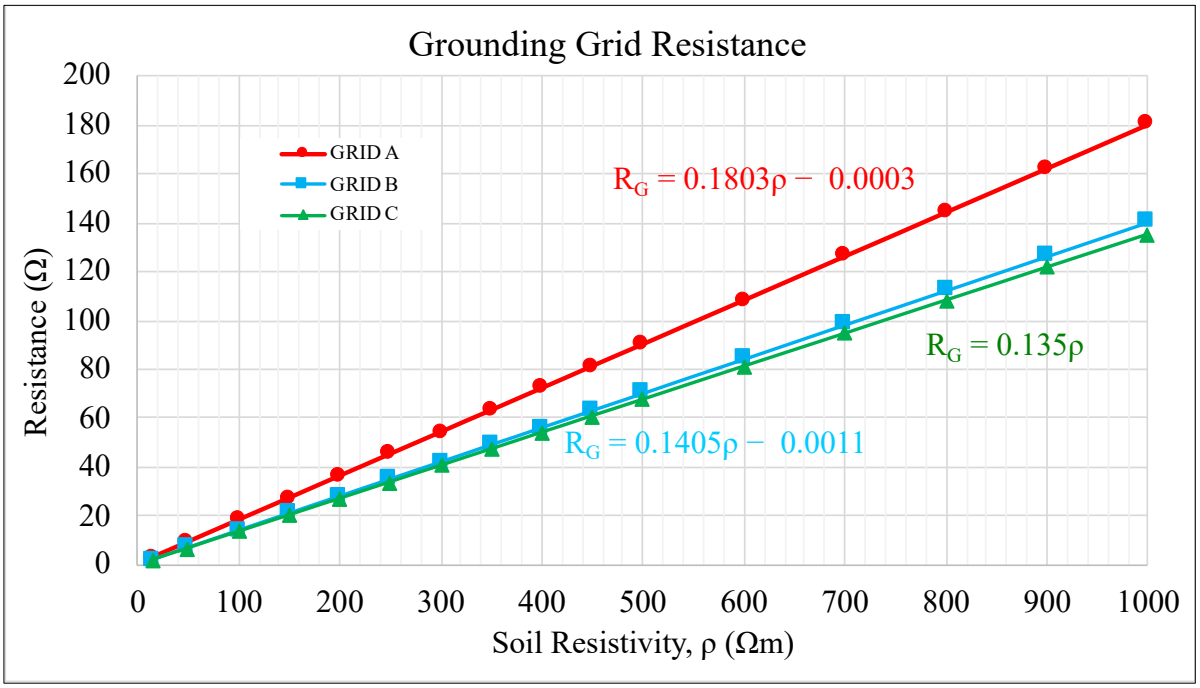

Figure 10. Grounding grid total resistance.

Additionally, this study evaluates the developed touch voltages across the grounding grids by comparing them with the safety voltage thresholds as shown in Figure 11. Notably, the investigation focuses on scenarios involving SC incidences at the middle of the MV line (L = 10 km). It is crucial to underscore the importance of the absence of hazardous developed potentials within the center of the grounding grids, particularly in proximity to the metallic control panel of the protection device.

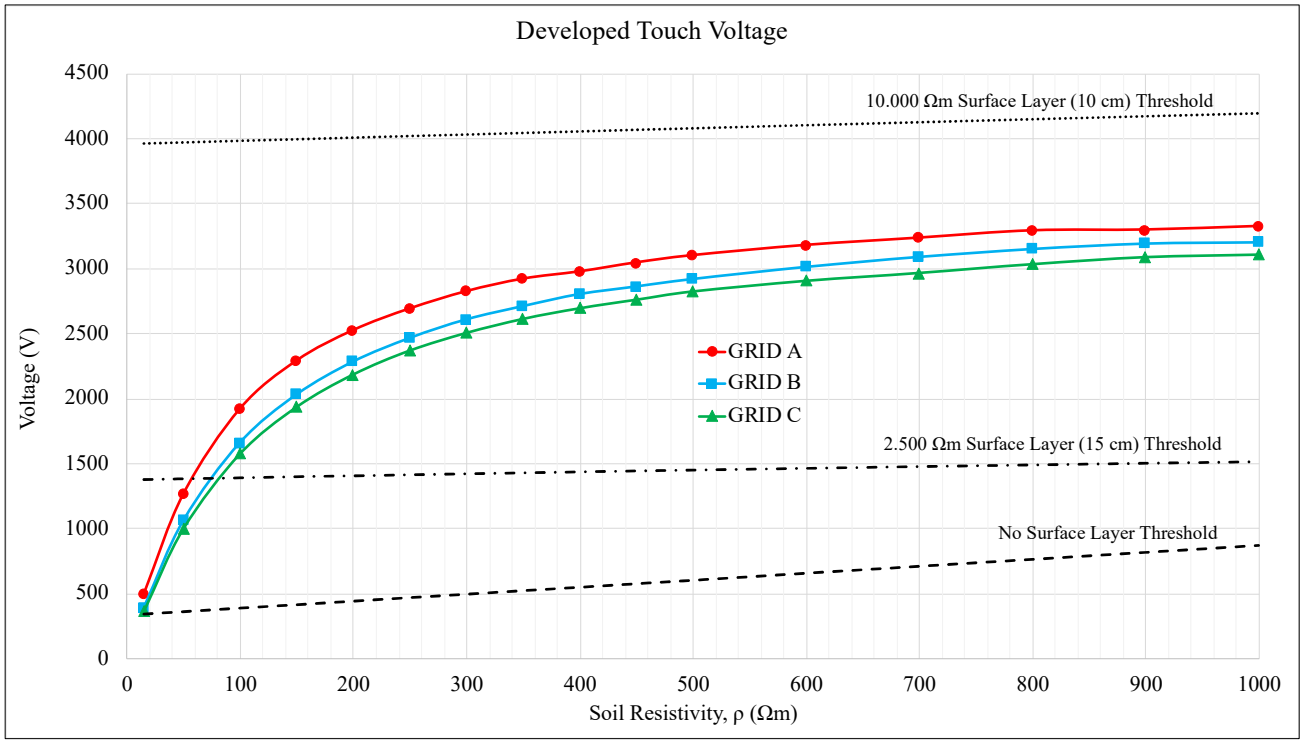

Figure 11. Developed touch voltage and safety thresholds (0.15 s faut clearing time).

As depicted in Figure 11, the developed touch voltage exceeds the safety threshold for all three grounding grids across the entire range of soil resistivities exceeding approximately 15 Ωm. However, upon the introduction of a surface layer characterized by high resistivity (ρ = 2.500 Ωm with at least 15 cm thickness), the grounding grids demonstrate improved protective capabilities, extending up to approximately 100 Ωm. Furthermore, a surface layer with an exceptionally high value of soil resistivity guarantees sufficient protection against developed touch voltages across the entire spectrum of soil structures for all three grounding grids. The following equations describe the trendlines modeling the developed touch voltages across the three variations of the grounding grid.

$$\text{GRID A}: \; V_t = 700 \cdot \ln(\rho) - 1300 \tag{5}$$

$$\text{GRID B}: \; V_t = 711 \cdot \ln(\rho) - 1546 \tag{6}$$

$$\text{GRID C}: \; V_t = 694 \cdot \ln(\rho) - 1540 \tag{7}$$

In Figure 12, the distribution of step and touch voltages across the surface of GRID A is depicted under several variations regarding the top layer surface. These variations are pertinent to an SC event occurring at the middle of the MV line, assuming a uniform soil structure with soil resistivity of 300 Ωm. This value is considered as an average worst-case scenario, which is subject to seasonal variations and the depth at which the grounding grid is placed beneath the Earth's surface. It is essential to highlight that regions represented by color gradients denote areas deemed unsafe, wherein the developed voltage surpasses the safety thresholds, while colorless regions signify safety compliance.

Moreover, in Figure 13, the distribution of step and touch voltages for GRID B and GRID C is depicted, incorporating an insulating surface layer composed of asphalt (ρ = 10.000 Ωm).

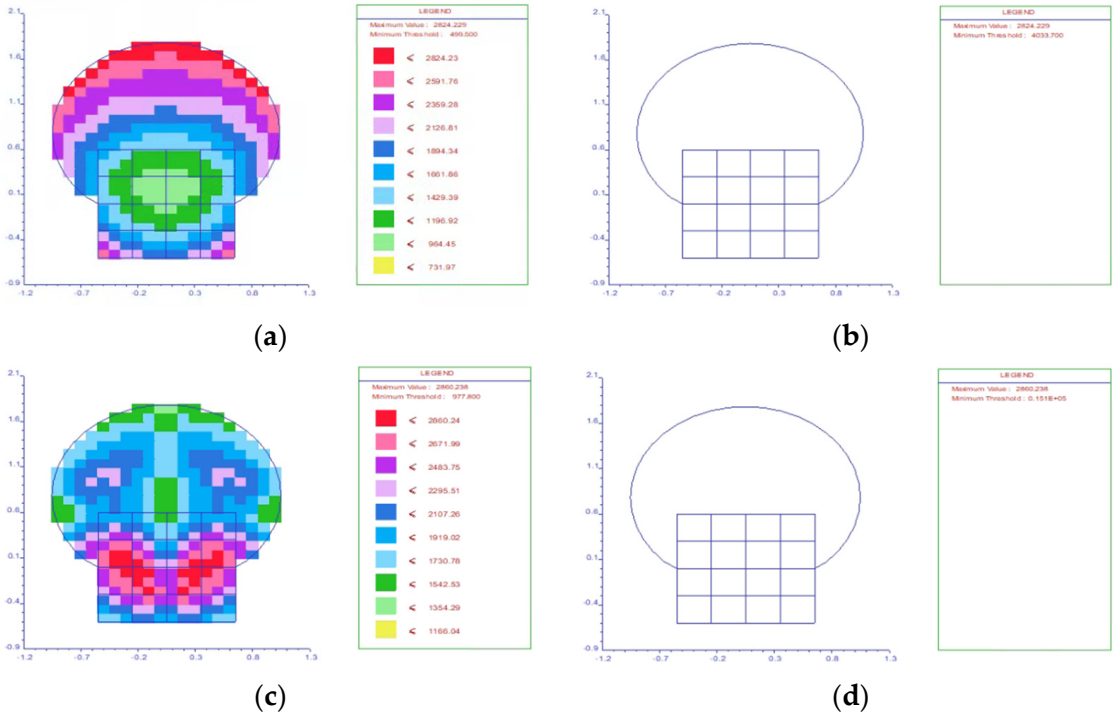

Figure 12. Developed potentials when a fault occurs on the middle of the MV line (L = 10 km) of GRID A (**a**) touch voltage without surface layer, (**b**) touch voltage with surface layer (10 cm) of high resistivity, ρ =10.000 Ωm, (**c**) step voltage without surface layer, and (**d**) step voltage with surface layer (10 cm) of high resistivity, ρ = 10.000 Ωm.

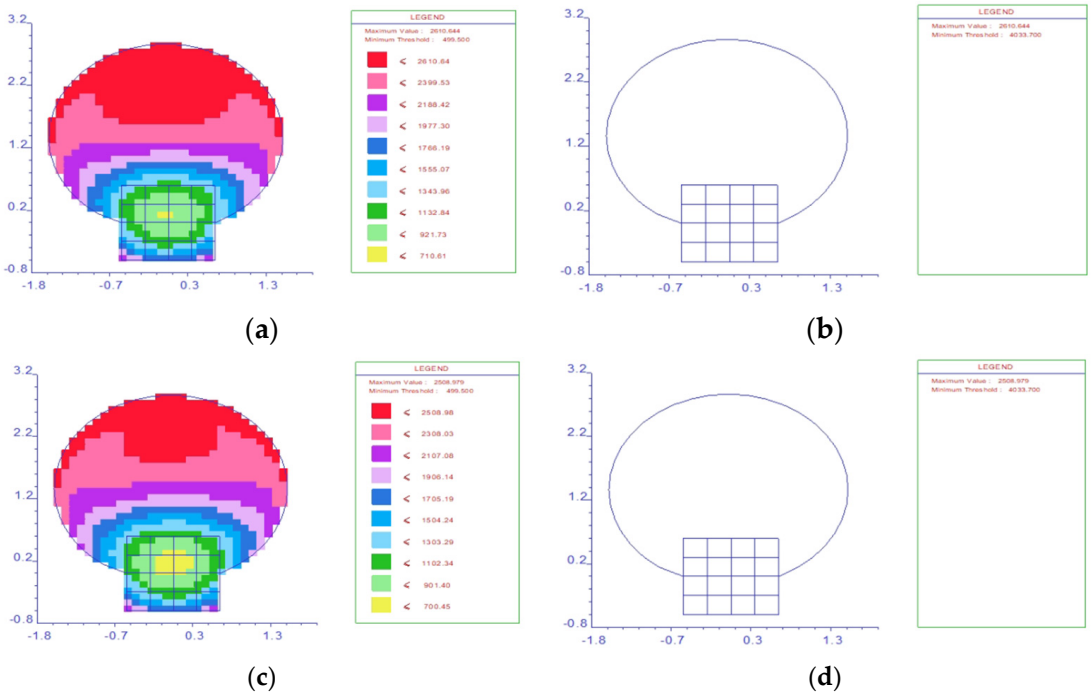

Figure 13. (**a**) Developed touch voltage when a fault occurs on the middle of the MV line (L = 10 km) of GRID B without surface layer, (**b**) developed step voltage of GRID B with surface layer of high resistivity, ρ = 10.000 Ωm, (**c**) developed touch voltage of GRID C without surface layer, and (**d**) developed touch voltage of GRID C with surface layer of high resistivity, ρ = 10.000 Ωm.

For a more detailed analysis, Appendix A presents detailed results of the developed touch and step voltages across all three variants of the grounding grid, considering a horizontal two-layer soil structure. It is noteworthy that this soil structure model offers enhanced accuracy, mirroring the real-world scenario where soil typically comprises multiple layers with varying resistivity.

5. Discussion

The current paper delves into the calculation of developed hazardous potentials resulting from a single-line-to-ground fault in the vicinity of an MV concrete pole. Through a comprehensive study of alternative scenarios, the study emphasizes the critical need for a detailed analysis of system configurations to mitigate consequences and safeguard human life from the risks posed by an inefficient grounding system. The acquired knowledge regarding the impact of various parameters on the performance of the MV grounding grids provides guidelines for engineers in making informed decisions during system design. The accurate evaluation of the performance of such installations is extremely crucial in ensuring MV networks' reliable and safe operation. The discussion of various design choices aims to develop a more detailed understanding of the performance of grounding systems in concrete poles, with an emphasis on safety. The analysis underscores the influence of factors such as distance from the HV/MV substation, grounding system design, soil resistivity, and an insulating surface layer on the magnitude of developed potentials. Notably, an increase in distance from the substation induces a reduction in potential values. Moreover, an insulation surface layer with high resistivity demonstrates a substantial reduction in developed potentials.

6. Conclusions

The primary objective of this analysis was to provide insights concerning the operational efficacy of grounding systems of MV concrete poles facilitating interconnections between overhead and underground sections of power distribution networks via switching devices. Additionally, the goal was to examine and propose possible alternatives and improvements to the existing grounding systems. Through extensive simulations, the following key conclusions emerged:

- In general, all examined grounding grids have a relatively dense design featuring a 4×4 grid.
- The efficacy of grounding systems is heavily contingent upon their installation location across the MV line. Notably, when an SC event occurs at a substantial distance from the HV substation, the resultant SC current is diminished. Consequently, grounding grids exhibit higher efficacy in mitigating the risk of hazardous touch and step voltages.
- For all three grounding grids, operating on a uniform soil structure, a linear correlation exists between the total grounding grid resistance and the soil resistivity, as depicted in Figure 10.
- Regarding the GRID B alternative, enlarging the radius of the circular loop results in a lower resistance and, therefore, a slightly better performance when compared to GRID A. However, it should be noted that due to its dense and small design it is still ineffective in providing adequate protection against hazardous potentials.
- Regarding GRID C, the incorporation of a grounding rod correlates with a notable 25% reduction in the maximum developed touch and step voltages, as depicted in Figure 11.
- All three grounding grid variations exhibit similar behavior regarding touch and step voltages; as such, they are ineffective in providing adequate protection against hazardous potentials. Therefore, it is imperative to incorporate a surface layer with high resistivity, ideally 2.500 Ωm with at least 15 cm thickness. To elaborate further, as illustrated in Figure 11, when the grounding grid is placed in farmlands with soil resistivity ranging from 200 to 300 Ωm, a top layer of 2.500 Ωm resistivity with thickness more than 15–20 cm is considered necessary. Conversely, in regions characterized

by high soil resistivity exceeding 200 Ωm, it is strongly recommended to incorporate a top layer of asphalt with a resistivity of 10.000 Ωm.

- All three grounding grid variations exhibit relatively high resistance, reaching 40 Ω when the soil resistivity is approximately 300 Ωm. This holds critical significance, as at this resistance level, the magnitude of the total fault current diminishes significantly. Consequently, the overcurrent relay positioned at the departure point of the HV substation may fail to detect the fault for tripping purposes. Such a fault scenario could potentially evolve into a permanent fault, posing substantial risks to the safety of personnel and passersby. It is therefore imperative to avoid placing the grounding grid in soil structures with resistivity exceeding 300 Ωm.
- If the fault clearing time exceeds the instantaneous operation of the circuit breaker (150 ms), the effectiveness of the grounding grids deteriorates significantly. One viable solution under such circumstances may be the addition of a top layer of asphalt.
- Based on the findings extracted from Tables A1–A3 in Appendix A, pertaining to a two-layer horizontal soil structure, it is evident that hazardous potentials (touch and step voltages) exhibit an upward trend with increasing soil resistivity in the upper layer. This phenomenon predominantly arises due to the positioning of the circular grounding grid loops within the upper layer, with only the grounding rods extending into the second layer. Consequently, when deploying grounding grids, DSOs should conduct comprehensive assessments of soil resistivity and ensure appropriate installation in the layer with the lowest possible soil resistivity.

Drawing from the simulation results, the paper advocates for an optimal approach to safeguarding personnel and passersby from hazardous voltages during a line-to-ground fault. This entails the installation of one of the three examined grounding models in conjunction with a surface layer of asphalt (ρ = 10.000 Ωm). Alternatively, if implementing such a solution proves impractical, it is recommended to consider adopting GRID C in conjunction with a surface layer featuring a resistivity ρ of 2.500 Ωm and substantial thickness. In summary, the extracted results from this study are anticipated to provide valuable support for the optimal design and implementation of an effective connection between overhead and underground systems. By endorsing safe and uninterrupted operation, these findings contribute significantly to enhancing the overall reliability and security of MV distribution systems.

Author Contributions: Conceptualization, E.D.E. and V.T.K.; methodology, E.D.E. and V.T.K.; software, G.L.; validation, E.D.E. and C.A.C.; formal analysis, C.A.C. and V.T.K.; investigation, E.D.E.; data curation, C.A.C. and I.F.G.; writing—original draft preparation, G.L. and E.D.E.; writing—review and editing, I.F.G.; visualization, E.D.E.; supervision, I.F.G.; project administration, I.F.G. All authors have read and agreed to the published version of the manuscript.

Funding: This research received no external funding.

Institutional Review Board Statement: Not applicable.

Informed Consent Statement: Not applicable.

Data Availability Statement: Dataset available on request from the authors.

Conflicts of Interest: The authors declare no conflicts of interest.

Appendix A

Table A1. Developed potentials for GRID A and horizontal two-layer soil structure without surface layer.

Soil Resistivity		Total Grounding Resistance	Touch Voltage Threshold	Step Voltage Threshold	L = 0 km			L = 10 km			L = 20 km		
ρ_1 (Ωm)	ρ_2 (Ωm)	R (Ω)	$E_{touch70}$ (V)	E_{step70} (V)	I_f (A)	V_t (V)	V_s (V)	I_f (A)	V_t (V)	V_s (V)	I_f (A)	V_t (V)	V_s (V)
100	250	26.2	393	552	302	1839.3	1974.7	276	1681.1	1804.7	248	1510.4	1621.6
	500	34.3	393	552	249	1584.9	1763.9	232	1476.7	1643.5	213	1355.7	1508.8
	750	39.6	393	552	224	1454.5	1645.3	210	1363.6	1542.5	135	1266.2	1432.3
	1000	43.4	393	552	208	1362.6	1557.7	197	1290.6	1475.3	185	1212	1385.5
	2000	53.5	393	552	176	1175.9	1365.5	168	1122.5	1303.5	159	1062.3	1233.6
250	100	32.6	473	871	259	3419.6	3243.9	240	3168.7	3006.0	220	2904.7	2755.58
	500	59.9	473	871	161	2410.8	2553.1	154	2306.1	2442.1	146	2186.2	2315.2
	750	70.3	473	871	140	2159.3	2343.1	135	2082.2	2259.4	130	3205.1	2175.7
	1000	78.9	473	871	127	1995.4	2197.8	123	1932.5	2128.6	118	1854.0	2042.1
	2000	101.1	473	871	101	1643.9	1852.3	99	1611.3	1826.7	97	1578.8	1789.8
500	100	54.5	605	1402	174	4420.8	4054.3	166	4217.5	3867.6	157	3988.9	3657.9
	250	70.0	605	1402	141	3782.1	3636.1	136	3648.1	3507.1	130	3787.1	3352.3
	750	106.4	605	1402	97	2840.9	2949.8	95	2782.3	2888.4	93	2723.7	2817.6
	1000	119.7	605	1402	88	2635.4	2790.9	86	2575.5	2727.3	84	2515.6	2664.1
	2000	157.7	605	1402	68	2136.8	2353.6	67	2105.4	2319.1	66	2073.9	2284.4
1000	100	97.0	871	2465	106	5255.3	4713.7	103	5106.6	4580.3	100	4957.8	4446.9
	250	114.6	871	2465	91	4673.9	4327.8	89	4571.2	4232.7	87	4468.4	4137.6
	500	139.9	871	2465	76	4077.1	3919.7	75	4023.5	3868.1	74	3969.8	3816.5
	750	161.7	871	2465	66	129	2049.4	2094.9	125	1985.9	2029.5	120	1906.4
	2000	239.4	871	2465	46	80	2289.8	2453.5	80	2289.8	2453.5	80	2289.8

Table A2. Developed potentials for GRID B and horizontal two-layer soil structure without surface layer.

Soil Resistivity		Total Grounding Resistance	Touch Voltage Threshold	Step Voltage Threshold	L = 0 km			L = 10 km			L = 20 km		
ρ_1 (Ωm)	ρ_2 (Ωm)	R (Ω)	$E_{touch70}$ (V)	E_{step70} (V)	I_f (A)	V_t (V)	V_s (V)	I_f (A)	V_t (V)	V_s (V)	I_f (A)	V_t (V)	V_s (V)
100	250	21.2	393	552	347	1601.3	1801.3	312	1433.7	1619.6	276	1273.6	1432.7
	500	28.6	393	552	284	1362.4	1629.1	261	1252.1	1497.1	237	1136.9	1359.5
	750	33.6	393	552	253	1232.6	1516.1	235	1144.95	1408.6	216	1052.4	1294.7
	1000	37.3	393	552	234	1152.2	1437.6	219	1078.3	1345.5	203	999.5	1247.2
	2000	47.0	393	552	319	1591	2051	185	923.2	1189.8	174	868.3	1119.1
250	100	24.5	473	871	316	3390.7	2995.4	287	3079.6	2721.0	256	2746.9	2427.1
	500	48.0	473	871	192	2184.1	2399.2	182	2070.3	2274.3	171	1945.1	32,136
	750	57.4	473	871	166	1937.2	2217.4	159	1855.5	2123.9	151	1762.2	2017.1
	1000	65.3	473	871	149	1766.1	2075.5	144	1706.9	2005.9	137	1623.9	1908.4
	2000	86.1	473	871	118	1440.6	1779.2	114	1391.8	1718.9	110	1342.9	1658.6
500	100	40.4	605	1402	220	4764	3845	207	4482.5	3618.2	193	4179.3	3373.5
	250	53.1	605	1402	177	3782.4	3468.8	169	3611.4	3312.3	160	3419.1	3135.6
	750	84.3	605	1402	120	2678.2	2851.3	116	2588.9	2756.2	112	2499.6	2661.2
	1000	96.0	605	1402	107	2434.3	2674.1	104	2366	2599.2	101	2297.8	2524.2
	2000	130.5	605	1402	80	1896.5	2228.7	79	1872.8	2200.9	78	1849.1	2173
1000	100	71.1	871	2465	140	6087.9	4660.9	134	5827	4460.9	128	5566.1	4261.2
	250	85.3	871	2465	119	5141.9	4255.9	115	4963.1	4112.3	111	4796.2	3969.8
	500	106.2	871	2465	97	4145.6	3802.1	95	4060.1	3723.6	93	3974.7	3645.2
	750	124.4	871	2465	85	3612.8	3564.1	83	3527.8	3480.2	81	3442.7	3396.4
	2000	192.1	871	2465	57	2593.5	2849.1	56	2548.1	2799.1	55	2502.5	2749.1

Table A3. Developed potentials for GRID C and horizontal two-layer soil structure without surface layer.

Soil Resistivity		Total Grounding Resistance	Touch Voltage Threshold	Step Voltage Threshold	L = 0 km			L = 10 km			L = 20 km		
ρ_1 (Ωm)	ρ_2 (Ωm)	R (Ω)	$E_{touch70}$ (V)	E_{step70} (V)	I_f (A)	V_t (V)	V_s (V)	I_f (A)	V_t (V)	V_s (V)	I_f (A)	V_t (V)	V_s (V)
100	250	20.9	393	552	350	1571.9	1775.5	315	1414.7	1597.9	278	1248.5	1410.2
	500	28.5	393	552	283	1338.1	1602.6	262	1238.8	1483.6	237	1120.6	1342.1
	750	33.5	393	552	253	1223.1	1505.6	236	1140.8	1404.4	216	1044.2	1285.4
	1000	37.2	393	552	235	1148.8	1436.4	219	1070.6	1338.6	203	992.4	1240.8
	2000	47.0	393	552	196	976.1	1257.5	185	921.3	1186.9	174	866.6	1116.3
250	100	21.7	473	871	342	2959.6	2760.7	309	2674.2	2494.3	273	2362.5	2203.7
	500	47.2	473	871	195	2144.2	2367.8	185	2034.3	2247.3	174	1913.3	2113.6
	750	56.8	473	871	168	1914.4	2201.9	160	1823.5	2097.5	152	173.4	1992.2
	1000	64.8	473	871	150	1745.5	2056.5	144	1675.6	1974.1	138	1605.9	1892.0
	2000	85.9	473	871	118	1429.3	1765.4	3114	1380.8	1705.5	111	1344.5	1660.7
500	100	330.9	605	1402	269	3981.9	3422.6	249	33,685.8	3168.1	227	3360.2	2888.2
	250	48.2	605	1402	192	3454.1	3311.9	182	3274.2	3139.4	171	3076.3	2949.6
	750	82.3	605	1402	122	2601.2	2788.2	119	2537.2	2719.7	114	2430.6	2605.4
	1000	94.4	605	1402	109	2397.1	2648.1	106	2331.1	2575.2	102	2243.2	2478.1
	2000	129.6	605	1402	82	1908.4	2248.5	80	1861.8	2193.6	78	1861.8	2193.6
1000	100	42.5	871	2465	212	4834.6	3949.2	200	4560.9	3725.6	186	4241.7	3464.9
	250	69.1	871	2465	142	4466.4	3926.1	137	4309.1	3787.8	131	4120.4	3621.9
	500	96.5	871	2465	106	3813.9	3656.9	104	3741.9	3587.9	100	3592.1	3449.9
	750	117.4	871	2465	89	3447.7	3429.4	87	3370.3	3352.3	85	3292.8	3275.3
	2000	188.8	871	2465	57	2507.1	2769.6	57	2507.1	2769.6	56	2463.1	2721.1

Table A4. Developed potentials for GRID A and uniform soil structure without surface layer.

Soil Resistivity	Total Grounding Resistance	Touch Voltage Threshold	Step Voltage Threshold	L = 0 km			L = 10 km			L = 20 km		
ρ (Ωm)	R (Ω)	$E_{touch70}$ (V)	E_{step70} (V)	I_f (A)	V_t (V)	V_s (V)	I_f (A)	V_t (V)	V_s (V)	I_f (A)	V_t (V)	V_s (V)
15	2.7	348	372	781	660.4	668.8	591	499.7	506.1	446	377.1	381.9
50	9.0	366	466	548	1544.6	1564.3	450	1268.4	1284.5	372	1048.5	1061.9
100	18.0	393	552	384	2164.7	2192.3	341	1922.3	1946.8	296	1668.6	1689.9
150	27.0	419	659	296	2502.9	2534.8	271	2291.6	2320.7	244	2063.2	2089.5
200	36.1	446	765	240	2705.8	2740.3	224	2525.4	2557.6	207	2333.7	2363.5
250	45.1	473	871	202	2846.7	2883.1	191	2691.4	2726.1	179	2522.6	2554.8
300	54.1	499	977	175	2959.5	2997.2	167	2824.1	2860.2	158	2672	2706.1
350	63.1	526	1084	154	3038.4	3077.2	148	2920	2957.3	141	2781.6	2817.4
400	72.1	552	1190	137	3089.1	3128.6	132	2976.4	3014.4	127	2863.7	2900.2
450	81.1	579	1296	124	3145.5	3185.6	120	3044.8	3082.9	116	2942.6	2980.1
500	90.1	605	1402	113	3185	3225.6	110	3100.8	3140.0	106	2987.7	3025.8
600	108.2	659	1615	96	3247	3288.4	94	3179.3	3220	91	3079.9	3117.6
700	126.2	712	1828	84	3314.7	3356.9	82	3235.7	3277	80	3156.8	3197.1
800	144.2	765	2040	74	3337.2	3379.7	73	3292	3334	71	3202	3242.7
900	162.3	818	2253	66	3348.5	3391.2	65	3297.8	3339.8	64	3247	3288.4
1000	180.3	871	2465	60	3382.3	3425.4	59	3325.9	3368.3	58	3269.6	3311.2

References

1. IEA. *Electricity Market Report 2023*; IEA: Paris, France, 2023; Available online: https://www.iea.org/reports/electricity-market-report-2023 (accessed on 25 April 2024).
2. IEA. *Renewables 2023*; IEA: Paris, France, 2023; Available online: https://www.iea.org/reports/renewables-2023 (accessed on 25 April 2024).
3. Alam, M.S.; Al-Ismail, F.S.; Salem, A.; Abido, M.A. High-Level Penetration of Renewable Energy Sources into Grid Utility: Challenges and Solutions. *IEEE Access* **2020**, *8*, 190277–190299. [CrossRef]
4. Loumakis, S.; Giannini, E.; Maroulis, Z. Renewable Energy Sources Penetration in Greece: Characteristics and Seasonal Variation of the Electricity Demand Share Covering. *Energies* **2019**, *12*, 2441. [CrossRef]
5. Ellinas, E.D.; Christodoulou, C.A.; Gonos, I.F. Medium voltage outdoor compact substations' earthing system evaluation based on quantified risk analysis. *Sustain. Energy Grids Netw.* **2023**, *36*, 101180. [CrossRef]
6. Poulimenos, G.A.; Ellinas, E.D.; Voumvoulakis, E.M.; Christoforos, S.T.; Christodoulou, C.A.; Gonos, I.F. Evaluation of the solid-state breakers on the performance of power distribution grids with high-RES penetration. *Electr. Power Syst. Res.* **2023**, *223*, 109580. [CrossRef]
7. Ellinas, E.D.; Damianaki, K.D.; Christodoulou, C.A.; Voumvoulakis, E.M.; Gonos, I.F. Grounding system of medium voltage network with integrated distributed generation: Short-circuit analysis and calculation of the developed potentials. In Proceedings of the 22nd International Symposium of High Voltage Engineering, Xi'an, China, 21–25 November 2021.
8. Evgenidis, K.F.; Ellinas, E.D.; Christodoulou, C.A.; Gonos, I.F. Performance Evaluation of Grounding System of Overhead Medium Voltage Power Line embedded with RES Distributed Generation. In Proceedings of the 2022 IEEE International Conference on High Voltage Engineering and Application (ICHVE), Chongqing, China, 25–29 September 2022.
9. *IEEE Std 80-2013*; IEEE Guide for Safety in AC Substation Grounding. IEEE: New York City, NY, USA, 2013.
10. *ANSI/IEEE Std 81-2012*; IEEE Guide for Measuring Earth Resistivity, Ground Impedance and Earth Surface Potentials of a Grounding System. IEEE: New York City, NY, USA, 2012.
11. *IEC 61936-1*; Power Installations Exceeding 1 kV AC and 1.5 kV DC—Part 1: AC. IEC: Geneva, Switzerland, 2021.
12. *IEC 60479-1*; Effects of Current on Human Beings and Livestock—Part 1: General Aspects. IEC: Geneva, Switzerland, 2018.
13. Qian, W.; Jun, L.; Jiandong, D.; Wangjing, T. Analysis of the impact of distributed generation on grounding method of distribution network. *J. Eng.* **2017**, *2017*, 907–910. [CrossRef]
14. Dong, L.; He, L.; Pu, T.-J. Effect of neutral grounding mode on reliability of distribution network. *Power Syst. Prot. Control* **2013**, *41*, 96–101. [CrossRef]
15. Sallam, A.A.; Malik, O.P. Earthing of Electric Distribution Systems. In *Electric Distribution Systems*; IEEE: New York City, NY, USA, 2019; pp. 73–109.
16. Datsios, Z.G.; Mikropoulos, P.N. Safety performance evaluation of typical grounding configurations of MV/LV distribution substations. *Electr. Power Syst. Res.* **2017**, *150*, 36–44. [CrossRef]
17. Guizán, R.; Colominas, I.; París, J.; Couceiro, I.; Navarrina, F. Numerical analysis and safety design of grounding systems in underground compact substations. *Electr. Power Syst. Res.* **2022**, *203*, 107627. [CrossRef]
18. da Silva, L.N.; Djambolakdjian, G.S.; da Silva Gazzana, D.; Ferraz, R.G.; Vidor, F.F. Underground Substation Grounding Evaluation Using the Average Potential Method. In Proceedings of the 2022 IEEE International Conference on Environment and Electrical Engineering and 2022 IEEE Industrial and Commercial Power Systems Europe (EEEIC/I&CPS Europe), Prague, Czech Republic, 28 June–1 July 2022; pp. 1–5.
19. Colominas, I.; París, J.; Guizán, R.; Navarrina, F.; Casteleiro, M. Numerical Modeling of Grounding Systems for Aboveground and Underground Substations. *IEEE Trans. Ind. Appl.* **2015**, *51*, 5107–5115. [CrossRef]
20. *EN 50341-1:2012*; Overhead Electrical Lines Exceeding AC 1 kV-Part 1: General Requirements-Common Specifications. CENELEC: Bruxelles, Belgium, 2012.
21. Singh, M. Protection coordination in distribution systems with and without distributed energy resources—A review. *Prot Control Mod Power Syst.* **2017**, *2*, 27. [CrossRef]

22. *IEEE Std C37.2-2008*; IEEE Standard Electrical Power System Device Function Numbers, Acronyms, and Contact Designations. IEEE: New York City, NY, USA, 2008.
23. *IEC 60255-151:2009*; Measuring Relays and Protection Equipment—Part 151: Functional Requirements for over/under Current Protection. IEC: Geneva, Switzerland, 2009.
24. ABB: REF 610 Feeder Protection Relay' Buyer's Guide—ANSI Version. 2005. Available online: https://library.e.abb.com/public/95f5a8c1854273d8c12570b1004948ae/ref610_ANSItob_755574_ena.pdf (accessed on 25 April 2024).
25. *DIgSILENT Power Factory Documentation: ABB REF 610 Relay Model Description, Version 003; DIgSILENT GmbH: Gomaringen, Germany*.
26. DIgSILENT Power Factory: User Manual, Version. 2022. Available online: https://www.digsilent.de/en/downloads.html?folder=files/downloads/public/10_PowerFactory/20_What's+New (accessed on 25 April 2024).
27. SES & Technologies. CDEGS Software 2017 User Manual. 2017. Available online: https://www.sestech.com/common/distro_docs/17.0/PDF/GetStart.pdf (accessed on 25 April 2024).
28. Permal, N.; Osman, M.; Ariffin, A.M.; Kadir, M.Z.A.A. The Impact of Substation Grounding Grid Design Parameters in Non-Homogenous Soil to the Grid Safety Threshold Parameters. *IEEE Access* **2021**, *9*, 37497–37509. [CrossRef]